Preprints of the 19th World Congress
The International Federation of Automatic Control
Cape Town, South Africa. August 24-29, 2014

Set-membership fault detection under noisy environment in aircraft control surface servo-loops

Christophe Combastel, * **Rihab El Houda Thabet,** **
Tarek Raïssi, *** **Ali Zolghadri** ** **David Gucik** **

* *ENSEA, ECS-Lab, 6 Avenue du Ponceau, 95014 Cergy, France, (e-mail: christophe.combastel@ensea.fr)*
** *University of Bordeaux, IMS-CNRS, 351 cours de la libration, 33405 Talence, France, (e-mail: rihabelhouda.thabet@u-bordeaux1.fr, ali.zolghadri@ims-bordeaux.fr, david.gucik@ims-bordeaux.fr)*
*** *CNAM, CEDRIC-LAB, 292 rue Saint Martin, 75141 Paris, (e-mail: tarek.raissi@cnam.fr)*

Abstract: Based on a consistent interface between a data-driven and a model-driven approach within an interval framework, the paper deals with the detection of two important electrical flight control system failure cases of aircraft control surfaces, namely runaway and jamming. Robust and early detection of such abnormal positions is an important issue for early system reconfiguration and for achieving sustainability goals. The motivation behind this work is the development of an original set-membership methodology for fault detection where a data-driven characterization of random noise variability (which is not usual in a bounded error context) is combined with a model-driven approach based on interval prediction in order to improve the accuracy of the overall detection scheme. The efficiency of the proposed methodology is illustrated through simulation results using data sets recorded on a highly representative aircraft benchmark.

Keywords: Fault detection; Flight Control System; Set-membership; Uncertainty; Robustness

1. INTRODUCTION

For overall aircraft optimization design, early and robust detection of faults that may have an influence on structural loads is a challenging issue, as it can contribute to weight saving for better overall performance in terms of fuel burn, noise, range and environmental footprint, see for example Zolghadri et al. (2013). In this paper, a set membership methodology based on interval techniques to compute robust adaptive thresholds is proposed for fault detection of two important electrical flight control system failure cases of aircraft control surfaces: runaway and jamming. A runaway is an unwanted, or uncontrolled, control surface deflection that can go until the moving surface stops if it remains undetected. A jamming, or lock-in-place failure, is a generic system-failure case which generates control surface stuck at its current position.

Popular design methods for model-based Fault Detection and Diagnosis (FDD) include nonlinear, hybrid or unknown input observers, parity checks, parametric approaches, nonlinear local filtering, geometric methods, sliding mode methods etc. See for example Hwang et al. (2010); Ding (2008) and Zolghadri (2012) for a survey.

Model-based detection of runaways and jammings has been reported in several recent works. In Kim et al. (2008) an interacting multiple model filter for actuator fault detection was proposed which can diagnose the actuator damage with an unknown magnitude. In Han et al. (2012) a fault detection and isolation (FDI) algorithm was proposed for the stuck fault detection of an aircraft with multiple control surfaces. It relies on the joint use of an adaptive observer designed for the stuck fault detection, and a kalman filter based bias estimation identifying the stuck position of the corresponding control surface. In Varga et al. (2011) the authors developed a residual generator based on Linear Parameter-Varying (LPV) models which has been applied to the same application as in this paper. In Vanek et al. (2011) a geometric fault detection approach was proposed and applied to aileron actuator fault. In Henry et al. (2011) a LPV technique is proposed for aileron jamming, runaway and disconnection. In Gheorghe et al. (2013) a Kalman-based strategy was applied. In Efimov et al. (2011), a high-order sliding mode differentiation technique has been proposed.

In this paper, the proposed methodology is based on a data-driven characterization of variability (inherent randomness) and a model-based dynamic propagation of imprecision (lack of knowledge) to improve the detection accuracy (Aughenbaugh and Paredis (2006)). In fact, an original noise characterization capturing more information than just bounds at a given time instant will be taken into

⋆ This work is done within the MAGIC-SPS project (Guaranteed Methods and Algorithms for Integrity Control and Preventive Monitoring of Systems) funded by the French National Research Agency (ANR) under the decision ANR2011-INS-006.

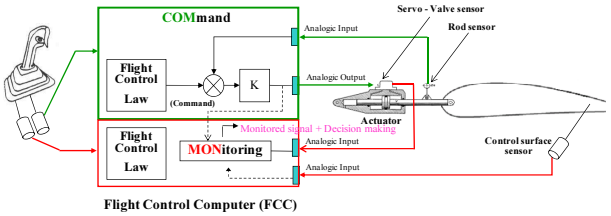

Fig. 1. Simplified block diagram of control surface servo-loop.

account, which is not usual in a bounded error context. This makes it possible to enhance the tradeoff between sensitivity to faults and robustness wrt noise. The resulting fault detection methodology relies on a distinction between signal and noise within measurements. This analysis results in the introduction of an interval residual based on a dead-zone function in order to interface the data-driven and the model-driven approaches. So, the proposed fault detection scheme takes into account both the inherent randomness of noise and the (non random) imprecision related to the lack of knowledge about the system dynamics.

The paper is organized as follows: section 2 is devoted to the problem statement and control surface servo loop modeling. The proposed fault detection methodology is described in section 3. Section 4 presents some simulation results. Finally, some concluding remarks are given in section 5.

2. PROBLEM STATEMENT

2.1 Basic physical model of the fault free system

A typical Airbus structure of servo-loop control of aircraft moving surfaces is depicted in figure 1 Goupil (2011). Here COM is the command channel and MON is the monitoring channel in the FCC (Flight Control Computer), see Goupil (2011) for further details. The control surface considered in this paper is the elevator which is moved by an hydraulic actuator. The nonlinear model of the actuator is derived from physical consideration, i.e. the rod speed is a function of the hydraulic pressure delivered to the actuator and the forces applying on the control surface and reacted by the actuator. Then, from a basic physical model (Zolghadri et al. (2013); Goupil (2010)), a state space representation can be derived as:

$$\begin{cases} \dot{x}(t) = \gamma(u(t), x(t))(u(t) - x(t)), \\ y(t) = x(t), \end{cases} \tag{1}$$

$$\gamma(u(t), x(t)) = K_{ci} K \sqrt{\frac{S\Delta P(t) - F_{aero}(t)}{S\Delta P_{ref} + K_a(t)(K_{ci}K(u(t) - x(t)))^2}} \tag{2}$$

where x is the rod position (which can be converted into the control surface position using a monotonic static function), $\Delta P(t)$ is the hydraulic pressure delivered to the actuator, $F_{aero}(t)$ represents the aerodynamic forces applied on the control surface. Depending on the control surface, F_{aero} is a function of several flight parameters like e.g. Mach number, dynamic pressure, aerodynamic configuration, etc.... $K_a(t)$ is the actuator damping coefficient. S is the actuator piston surface area. ΔP_{ref} is the differential pressure corresponding to the maximum rod speed. $u(t)$ is the actuator command signal (pilot order). K is the servo control gain (see figure 1) and K_{ci} models the actuator servo-valve by converting the servo-loop current derived from the flight control law order in rod speed.

In (2), several terms are time-varying, in particular the aerodynamic force $F_{aero}(t)$. The rod position x being measured ($y = x$) through the surface position sensor and a known static function, a simplified model can be obtained by substituting y for x in $\gamma(u, x)$ (2).

2.2 Problem statement

The aim is to propose a bounded error detection methodology which combines:

i) An explicit *data-driven* characterization of the output *noise* variability (i.e. random behavior of noise),
ii) An interval residual generator characterizing the output *signal* imprecision within a *model-driven* approach relying on guaranteed enclosures,
iii) An overall fault detection scheme further illustrated on a specific aircraft control surface.

To develop the methodology for fault detection of an elevator, a Linear Parameter-Varying (LPV) discrete state space representation like (3), corresponding to a sampled approximation of the fault free model (1), is considered.

$$\begin{cases} x_{k+1} = g_k x_k + (1 - g_k) h_k u_k, \quad x_0 \in (x_0^c \pm x_0^r), \\ y_k = x_k + \eta_k, \end{cases} \tag{3}$$

$$g_k \in (g_k^c \pm g_k^r), \quad h_k \in (h_k^c \pm h_k^r), \quad \eta_k \in (0 \pm \eta_k^r) \tag{4}$$

$u_k \in \mathbb{R}$ is a known input, $x_k \in \mathbb{R}$ is the system state, $y_k \in \mathbb{R}$ is the output measurement and $\eta_k \in \mathbb{R}$ represents a bounded noise. $\pm$ is an operator returning an interval from its center (left) and its radius (right) like in $c \pm r = [c - r, c + r]$. The exponent notations c and r respectively refer to such center and (positive) radius. g_k and h_k are not exactly known: they are assumed to be bounded by time-varying intervals (4) with known centers and radii possibly expressed as non linear functions of a known scheduling vector $\theta_k \in \mathbb{R}^p$. Contrary to x_0 (initial state), g_k and h_k, it is worth noticing that no bound η_k^r is assumed *a priori* for the bounded noise η_k. This emphasizes the fact that a data-driven characterization of noise is to be further considered. The structure of the state equation in (3) emphasizes the distinction between g_k and h_k which, if constant, would respectively tune the time constant (discrete pole) and the static gain used to model the system. This distinction is important because a large uncertainty about g may significantly affect a fault detection residual during transient operation involved by input excitation, while preserving a very good precision during steady operation provided h is well-known. A suitable propagation of bounded uncertainties will take this into account.

3. PROPOSED APPROACH

In this section, a data-driven characterization of noise is firstly detailed. Secondly, a model-driven approach based on interval prediction is proposed. Finally, by combining the two methods, a fault detection methodology is given.

3.1 Data-driven evaluation of imprecision based on variability

3.1.1 Noise characterization

A characterization of variability of real valued discrete time signals like $u = (u_k)_{k\in K^*\subset\mathbb{Z}}$ based on moving averages $u_{k/q}$ over increasing temporal windows lengths q, where K^* may be finite or not (e.g. $K^* = \mathbb{Z}$). Here, it is assumed that characterization takes place at a present time $k = 0$ so that past time $k < 0$ refers to available data from past experience, whereas future time $k \geq 0$ refers to future of the signal u. A theoretical characterization of variability in the signal u is then defined as the function $\lambda(u) : \mathbb{N} \mapsto \mathbb{R}$, $q \to \lambda_q^*(u)$ where $\lambda_q^*(u)$ is:

$$\lambda_q^*(u) = \max_{k\in K^*} |u_{k/q}|, \quad u_{k/q} = \frac{1}{q}\sum_{\tau=k-q+1}^{k} u_\tau, \qquad (5)$$

It can be viewed as a modeling of the variability of the signal u as a constraint between the variables u_k. However, since all the future of u is not available, a practical characterization of variability in u is defined as: $\lambda(u) : Q \mapsto \mathbb{R}$, $q \to \lambda_q(u)$ where $Q = \{1, \ldots, \overline{q}\} \subset \mathbb{N}$ and $\lambda_q(u)$ is as in (6):

$$\lambda_q(u) = \max_{k\in K\subset(K^*\cap\mathbb{Z}^-)} \varsigma|u_{k/q}|, \qquad (6)$$

$$\forall q \in Q,\ \lambda_q^*(u) \leq \lambda_q(u), \qquad (7)$$

where ς is a safety factor (> 1) ensuring the practical validity of assumption (7) and K indexes the available past ($k \in \mathbb{Z}^-$) samples of u. (7) is a stationarity assumption stating that the characterization of variability in u performed on available (i.e. past) data still allows the inference of relevant information in the future. Here, the link with the stochastic context is very strong. From a practical point of view, the assumption (7) is well satisfied for stationary noisy (i.e. featuring randomness in their behavior) signals, *no matter how their probability density is distributed*. This motivates the study of a threshold evaluation after the filtering of a (noisy) signal u practically characterized as in (6)-(7). It should be mentioned that random signals u with non-stationary probability density functions can also be taken into account and will leads to robust decisions as long as the noise characterization $\lambda_q(u)$ remains valid. Regarding the proposed practical characterization of variability, the storage of $\{\lambda_q(u),\ q \in \{1, \ldots, \overline{q}\}\}$ for large $\overline{q}$ may require a non negligible memory space for some embedded applications. Then, a power regression giving parameters (α, β, γ) such that $\lambda_q(u) < \alpha q^\gamma + \beta$ can be used to drastically reduce the memory requirements while preserving very simple online computations.

Remark: A measure of variability based on the proposed data-driven signal characterization can be given as $\upsilon(u) = \frac{1}{\zeta(2)-1}\sum_{q\in Q}\left(1 - \frac{\lambda_q(u)}{\lambda_1(u)}\right)\frac{1}{q^2}$ where $\zeta(2) = \sum_{q=1}^{\infty}\frac{1}{q^2} = \frac{\pi^2}{6}$ (Riemann serie) and $Q = \mathbb{N}\backslash\{0\}$. The choice for such measure is not unique and it is motivated by normalized values between 0 and 1. The measure of variability expresses the decrease of moving averages maximum values wrt moving horizon length.

In this paragraph, an easily implementable data-driven characterization of (noisy) signals based on moving averages has been proposed. The related interpretations motivate a study of how to take variability into account in a bounded error context in order to increase the precision of predicted values.

3.1.2 Noise filtering and threshold evaluation

The filtering of a (noisy) signal u is considered in this paragraph and, based on a practical characterization of variability, $\lambda(u)$, the evaluation of a robust threshold enclosing the filter output is proposed. While preserving the full coverage of bounded error techniques under (5)-(7), it is shown that taking variability into account allows one a noticeable increase of precision when $\upsilon(u) > 0$.

Proposition 1. (Threshold evaluation by first order filtering). Let $u = (u_k)_{k\in\mathbb{N}}$ be a real scalar signal assumed to be characterized by $\lambda_q(u)$, $q \in Q = \{1, \ldots, \overline{q}\}$, $\overline{q} \in \mathbb{N}$. Let $r \in Q$ denote a number of past samples defining the history used for threshold evaluation. Let consider a first-order discrete filter (8)-(9) where, $\forall k \geq r$, $x_{k-r} \in (0 \pm \mu_{k-r}) \subset \mathbb{R}$, $0 < a < 1$, $b \geq 0$, $c \geq 0$:

$$x_k = ax_{k-1} + bu_k, \qquad (8)$$

$$y_k = cx_k, \qquad (9)$$

Then, $\forall k \geq r$, $|y_k| \leq \tau_{k,r}$, where the threshold $\tau_{k,r} = \tau(\lambda(u), r, \mu_{k-r}, a, b, c)$ is:

$$\tau_{k,r} = ca^r\mu_{k-r} + cbr(a^{r-1})\lambda_r(u) + cb\sum_{q=1}^{r-1} q(a^{q-1} - a^q)\lambda_q(u) \qquad (10)$$

(See Appendix for the proof). Let us now exemplify how proposition 1 can be used to achieve a robust residual evaluation in the context of fault detection. In order to follow the generic filtering notations of proposition 1, it is considered, in this paragraph only, that $u = (u_k)_{k\in\mathbb{N}}$ stands for a residual signal featuring some variability previously characterized by $\lambda_q(u)$, $q \in Q = \{1, \ldots, \overline{q}\}$, $\overline{q} \in \mathbb{N}$. In order to enhance the detection decision wrt to particular realizations of noise, residual are usually filtered prior to comparing them with some threshold. Therefore, let us consider the filtering of the (residual) signal u by a stable first-order discrete-time filter with unit static (e.g. $b = (1 - a)$, $c = 1$) gain and a as discrete pole ($0 < a < 1$). Such filter can be represented in state-space form as in (8)-(9) so that the output y has the meaning of a filtered residual signal. Then, a robust threshold signal τ enclosing y with guarantee provided the characterization of u remains valid is given as a corollary of proposition 1:

Corollary 2. Following all the assumptions of proposition 1 and assuming that u refers to a residual signal, $b = (1 - a)$, $c = 1$ (filter with unit static gain), $r = \min(k, \overline{q})$ and, $\forall k \in \mathbb{N}$, $\mu_{k-r} = \lambda_1(u)$. Then, a threshold signal τ enclosing the filtered residual y with guarantee provided the characterization $\lambda_q(u)$, $q \in Q = \{1, \ldots, \overline{q}\}$, $\overline{q} \in \mathbb{N}$ of u remains valid (7) is:

$$\forall k < \overline{q},\ |y_k| \leq \tau_k, \textit{with } \tau_k = \tau_{k,k}|_{\mu_{k-r}=\lambda_1(u)} \qquad (11)$$

$$\forall k \geq \overline{q},\ |y_k| \leq \tau_k, \textit{with } \tau_k = \tau_{k,\overline{q}}|_{\mu_{k-\overline{q}}=\lambda_1(u)} = \textit{constant} \qquad (12)$$

(See Appendix for the proof). It is worth underlining that τ is only variable for a short time of $\overline{q}$ samples from start-up of the (online) detection algorithm at $k = 0$. After that,

$\forall k \geq \overline{q}$, $\tau_k = \tau$ is a constant value (12) that can be easily pre-computed off-line from the characterization $\lambda(u)$ of the (residual) signal u as ($b = 1 - a$, $c = 1$):

$$\tau = a^{\overline{q}}\lambda_1(u) + (1-a)\left(\overline{q}(a^{\overline{q}-1})\lambda_{\overline{q}}(u) + \sum_{q=1}^{\overline{q}-1} q(a^{q-1} - a^q)\lambda_q(u)\right) \tag{13}$$

When $k \geq \bar{q}$ with sufficiently high $\bar{q}$ and $0 < a < 1$, the threshold τ is not much influenced by the (possibly high) maximum value $\lambda_1(u)$ of u at a single time instant. Instead, the decrease wrt q of moving average bounds $\lambda_q(u)$ characterizing a random signal u mainly contribute to a reduced (i.e. more sensitive) but still robust value of τ. Such robustness is guaranteed even under non-stationary stochastic properties of u provided the easily computable off-line characterization $\lambda_q(u)$ remains valid. This requires to learn the noise characterization based on data sets obtained from sufficiently excited scenarios with greatest noise levels under fault-free operation, as this will be done in section 4.

A systematic approach to compute thresholds based on an explicit data-driven characterization of (noisy) signals has been proposed, with no prior assumption about the probability density distribution of the sample values. Even if a significant part of such distribution is contained in the characterization $\lambda(u)$, the interest of the proposed scheme relies on the direct link between data-driven signal characterization and threshold evaluation, while still ensuring guaranteed robustness (complete coverage) under explicitly specified stationarity assumptions (7) which remain easily interpretable in terms of moving average.

Remark: When $v(u) = 0$ (signal with no variability), $\tau = \lambda_1(u)$ since $\forall q, \lambda_q(u) = \lambda_1(u)$, whereas $v(u) > 0$ (signal with explicit variability) leads to $\tau < \lambda_1(u)$ thanks to lower moving averages bounds as q increases. As expected, taking variability into account, which is not usual in a bounded error context, enhances the tradeoff between sensitivity to faults and robustness wrt noise

3.2 Model-driven interval prediction

Several works dealt with interval prediction mainly for LTI systems Mazenc and Bernard (2011); Combastel (2013); Mazenc et al. (2012). In addition, some results for interval observers for LPV systems, that can also be used for prediction, have been published in Gouzé et al. (2000); Raïssi et al. (2012). In this section, an interval prediction for the model (3)-(4) is given. The application under study leads us to focus on a first order model which formalizes prior knowledge about the dynamical behavior of the system to be further diagnosed.

Proposition 3. (Interval predictor). An interval predictor for the state equation in (3)-(4) and satisfying the guaranteed inclusion (16) is (14)-(15), where (17) ensures the stability of both the center (14) and the radius (15) dynamics.

$$x^c_{k+1} = g^c_k x^c_k + (1 - g^c_k)h^c_k u_k, \tag{14}$$

$$x^r_{k+1} = (|g^c_k| + g^r_k)x^r_k + g^r_k|x^c_k - h^c_k u_k| + (|1 - g^c_k| + g^r_k)h^r_k u_k \tag{15}$$

$$\forall k \in \mathbb{N},\ x_k \in x^c_k \pm x^r_k, \tag{16}$$

$$|g^c_k| + g^r_k < 1. \tag{17}$$

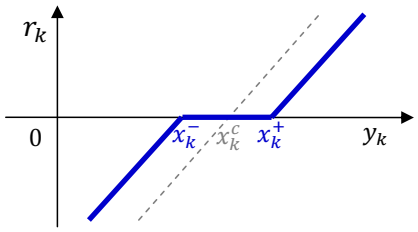

Fig. 2. Interval residual r_k based on a dead-zone function dz called with $[x^-_k, x^+_k] = x^c_k \pm x^r_k$.

(See Appendix for the proof). Notice that the condition (17) reduces to the LTI case when $g^c_k = g^c$ is constant and $g^r_k = 0$. Strong analogies exist with the stability condition given in Raka and Combastel (2013) for multi-dimensional continuous systems. An interesting aspect of proposition 3 is that it deals with a full time-varying bounded error LPV model including both time-varying centers *and* radii in the specification of parameters imprecision. In addition, it provides jointly: *i*) a guaranteed inclusion, *ii*) an easily verifiable stability condition for both center and radius dynamics, *iii*) a simple structure which is very well-suited for efficient real-time implementation.

3.3 Fault detection methodology

The fault detection methodology proposed in this work combines a model-driven approach as developed in section 3.2 and a data-driven approach as developed in section 3.1. A careful analysis of their interaction is investigated in this paragraph in order to achieve a robust and sensitive fault detection.

Firstly, based on the knowledge model (3), the interval predictor of proposition 3 gives $x^c_k \pm x^r_k$, a guaranteed interval prediction of the state x_k, which allows the explicit characterization of the influence of imprecisions about the system dynamics (lack of knowledge specified by g^r_k, h^r_k), even under arbitrary input excitation.

Secondly, based on the resulting bounds ($x^-_k = x^c_k - x^r_k$, $x^+_k = x^c_k + x^r_k$) and given the measurement equation of (3), an interval-based residual r_k can be defined as follows:

$$r_k = dz(y_k, x^c_k \pm x^r_k) = \begin{cases} y_k - x^+_k & \text{if } y_k > x^+_k, \\ y_k - x^-_k & \text{if } y_k < x^-_k, \\ 0 & \text{otherwise,} \end{cases} \tag{18}$$

(18) shows that $\forall y_k \in x^c_k \pm x^r_k$, $r_k = 0$ which is consistent with a measured value y_k belonging to its noise-free model-based interval prediction $x^c_k \pm x^r_k$. Otherwise, $\forall y_k \notin x^c_k \pm x^r_k$, $r_k \neq 0$, and the value of r_k is related to the distance between y_k and the closest bound of $x^c_k \pm x^r_k$. Consequently, the proposed deadzone-based residual evaluates the part of the measurement y_k that cannot be explained by the *interval* prediction resulting from the (noise-free) uncertain state equation in (3)-(4). Notice that the interval based residual is expressed as $r_k = r(y_k, x^c_k \pm x^r_k)$ (with $r = dz$) which is in contrast to the classical output error residual expressed as $\rho_k = \rho(y_k, x^c_k)$ ($= y_k - x^c_k$). This is illustrated by figure 2 where r (resp. ρ) appear with bold (resp. greyed dashed) lines. It is also worth noticing that $(x^r_k = 0) \Rightarrow (r_k = y_k - x^c_k = \rho_k)$ is satisfied which emphasizes the fact that the proposed interval

residual generalizes the classical one, the fit occurring when the knowledge is subject to full precision (i.e. no imprecision and thus zero radius).

Then, given a measurement and a set-membership estimation of the related measured variable, a residual quantifying the inconsistency between them is proposed. Under the assumption of validity of the fault-free model (3), the only cause of inconsistency ($r_k \neq 0$) is due to the unknown output error $\eta_k = y_k - x_k$ (unknown since x_k is not exactly known: $x_k \in x_k^c \pm x_k^r$). Notice that, at this step, η_k is not yet qualified as "noise", just as "output error". The reason comes from the lack of a clear distinction in an experimental context between *signal* and *noise* within a single observed reality which is the *measurement*.

In the proposed set-membership methodology, the disturbance bounds (g_k^r and h_k^r for model (4)) are viewed as a mean to model the frontier between what is considered as *noise* (and features a random behavior) and what is considered as *signal* in the *measurement*. A notable difference with usual practice is that this makes it possible to characterize the random behavior of noise through a data-driven approach and, in the same time, to specify a range of non-random dynamical behaviors handled by a guaranteed set-membership model-driven approach. By this way, it becomes possible to enclose within $x_k^c \pm x_k^r$ the influence of physical phenomena which are both non-random and whose precise modeling is not relevant for the considered application, while efficiently dealing with the noise in $r_k = dz(y_k, x_k^c \pm x_k^r)$ that remains unexplained by $x_k^c \pm x_k^r$. This is especially useful to maintain a robust decision both during large transients involved by input excitation under uncertain dynamics (g_k^r) and, in the same time, preserve the ability to "take robust decisions inside the noise" when x_k^r is very small (as in steady state for $h_k^c = 1$ and $h_k^r = 0$, for instance).

Thirdly, since the interval residual $r_k = dz(y_k, x_k^c \pm x_k^r)$ is only influenced by noise, the noise characterization and the filtered noise thresholding technique proposed in section 3.1 becomes readily applicable to achieve both sensitive and robust fault detection, even in the presence of large noise variability. Moreover, the proposed methodology does not require a new data-driven characterization to update the detection threshold when it is just decided to update the tuning of the residual filter.

4. SIMULATION RESULTS

In this section, some simulations results are presented to illustrate the methodology described in the previous section. First, the continuous time model (1) is transformed into a discrete time model:

$$g_k^c = (1 - \gamma(u_k, y_k, \theta_k)T), \quad h_k^c = 1, \tag{19}$$

where $T = 10$ ms is the sampling time. Then, the center dynamics (14) of the interval predictor resulting from the proposition 3 corresponds to the sampled approximation of the simplified model deduced from (1)-(2). g_k^r and h_k^r are tuned so that all non-modeled phenomena are well covered by $x_k^c \pm x_k^r$, up to (random) noise: $g_k^r = min(\kappa_1 + \kappa_2|u_k - x_k^c|, \kappa_3)$ where $\kappa = [\kappa_1, \kappa_2, \kappa_3] > 0$ is a vector of positive constants such that the stability condition (17) is satisfied under the considered domain of operation.

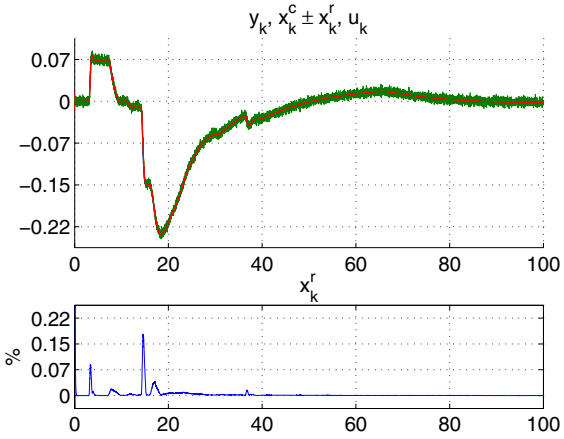

Fig. 3. Scenario $\mathcal{D}_\mathcal{V}$: Measured surface position y_k (green), bounds of its interval prediction $x_k^c \pm x_k^r$ (red) and actuator command signal (pilot order) u_k (blue). Bottom plot: x_k^r featuring increased values (i.e. reduced precision of the related interval prediction) during transient operation.

Based on the characterization of the variability in r_k computed from a first data set $\mathcal{D}_\mathcal{L}$ ($\mathcal{L}$ for learning), a threshold τ (13) is fixed for ε_k which results from the filtering of r_k by a first order discrete filter F_a with pole a ($0 < a < 1$) and unit static gain. Therefore, F_a has the form of (8) with $b = (1 - a)$, $c = 1$, and the threshold computation directly results from proposition 1 by taking r_k as input and ε_k as output. A fault is then detected once an inconsistency appears i.e. at the first sample time k such that $|\varepsilon_k| > \tau$. Notice that this condition implicitly involves a decision based on several samples of r_k thanks to the filtering process. A slow dynamic of the residual filter ($a \to 1$) is useful to improve the sensitivity to slowly developing abnormal behaviors with amplitude significantly smaller that the noise magnitude. The counterpart of this is a possibly slower detection delay in the case of abrupt faults since the filter output ε_k needs longer time to follow the filter input r_k.

This is illustrated on the considered system, by considering the data set $\mathcal{D}_\mathcal{V}$ used for a validation of the proposed methodology. This scenario $\mathcal{D}_\mathcal{V}$ features reduced input excitation magnitude (involving narrower control surface position range than $\mathcal{D}_\mathcal{L}$) and operates close to steady-state where random noise magnitude appears as the main difficulty to increase the sensitivity to faults (see figures 3). Notice that other scenarios with increased input excitation may lead to significantly larger intervals than in figure 4 during transient operation.

Based on the noise characterization learned with the excited scenario $\mathcal{D}_\mathcal{L}$, the fault-free scenario $\mathcal{D}_\mathcal{V}$ is taken as a reference for validation. Firstly, the noise characterization obtained from $\mathcal{D}_\mathcal{L}$ ensures no false alarms occur on the filtered residuals $a \in \{0.6, 0.8, 0.9, 0.95, 0.99\}$ (safety factor $\varsigma = 1.2$). Then, from the scenario $\mathcal{D}_\mathcal{V}$, three abnormal situations have been considered:

- $\mathcal{D}_{\mathcal{V}1}$: Runaway $-5°/s$ at $t = 50s$ (low dynamic runaway),
- $\mathcal{D}_{\mathcal{V}2}$: Jamming at $t = 14.5s$,
- $\mathcal{D}_{\mathcal{V}3}$: Jamming at $t = 66s$,

The fault detection results are reported in figure 5 and

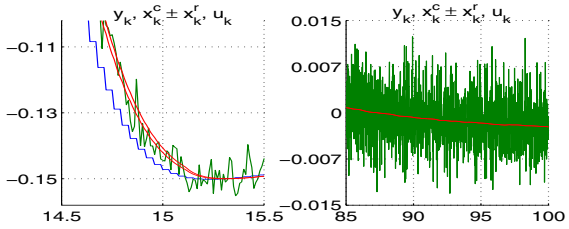

Fig. 4. Scenario $\mathcal{D}_\mathcal{V}$: Zoom of the top plot in figure 3 during transient operation (left) and during ≈steady-state operation (right).

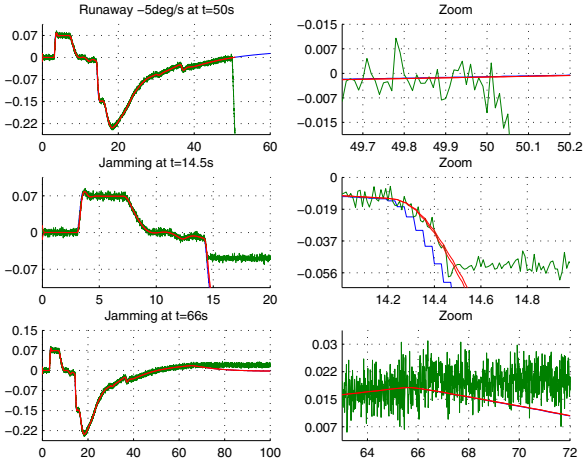

Fig. 5. Scenario $\mathcal{D}_\mathcal{V}$ under three distinct abnormal situations: $\mathcal{D}_{\mathcal{V}1}$, $\mathcal{D}_{\mathcal{V}2}$, $\mathcal{D}_{\mathcal{V}3}$, from top to bottom. Left: large view, Right: zoom around the times of fault occurrence and fault detection. All plots: Measured surface position y_k (green), bounds of its interval prediction $x_k^c \pm x_k^r$ (red) and actuator command signal (pilot order) u_k (blue).

table 1. In the scenario $\mathcal{D}_{\mathcal{V}1}$ (top plots in figure 5), the residual deviates abruptly from zero resulting in a fast detection. A similar situation can be observed $\mathcal{D}_{\mathcal{V}2}$ (middle plots in figure 5)). In both cases (runaway and jamming), an early fault detection is achieved as shown by the third and the fourth lines in table 1, except by the residual filter $a = 0.99$ which involves a very slow following of r_k by ε_k. The abnormal situation $\mathcal{D}_{\mathcal{V}3}$ corresponds to a jamming at a time ($t = 66s$) when the servo-loop operates approximately in steady-state. As the position changes slowly, the lock-in-place failure is more difficult to detect early, especially in the presence of noise which is not much a problem in the case of very abrupt faults. In that situation, residual filtering is of prior importance to both achieve an early detection. The third line in table 1 illustrates the trade-off in the choice on the residual filter dynamic ($a = 0.9$ or 0.95 being good candidates). Having a look at the bottom right plot in figure 5 the tradeoff sensitivity/robustness, the interest in taking the notion of signal variability in a bounded-error paradigm appears clearly. This study shows that the proposed set-membership methodology could allow the detection of runaway (a.k.a. hardover) and jamming (or lock-in-place failure) of aircraft control surfaces.

Table 1. Detection times (s) wrt residual filter pole a.

$a =$	0.6	0.8	0.9	0.95	0.99
$\mathcal{D}_{\mathcal{V}1}$: Run $t = 50s$	50.05	50.05	50.06	50.06	50.13
$\mathcal{D}_{\mathcal{V}2}$: Jam $t = 14.5s$	14.55	14.56	14.57	14.58	14.65
$\mathcal{D}_{\mathcal{V}3}$: Jam $t = 66s$	68.46	68.14	67.35	66.94	67.71

5. CONCLUDING REMARKS

In this work, a set-membership detection technique was proposed. The basic idea is to design interval residuals with a dead-zone function evaluating the behavior that cannot be explained by the set-membership model knowledge. Under fault free operation, such residuals are subject to deviations from zero induced by random noise only. The variability of such noise is characterized to obtain thresholds (intervals) accounting for both data-based and model-based knowledge. The technique has been applied to the detection of abnormal aircraft control positions. The obtained results are encouraging and open the door for further investigations in this direction.

Acknowledgement
The authors would like to thank Dr Philippe Goupil (AIRBUS Operations SAS, Toulouse, France) for his helpful comments.

APPENDIX

Proof. Proposition 1
By developing the recurrence (8) r times, it comes:
$x_k = a^r x_{k-r} + b(\, a^{r-1}u_{k-r+1} + a^{r-2}u_{k-r+2} + \ldots + a^1 u_{k-1} + a^0 u_k\,)$,
x_k is then rewritten so as to put into evidence cumulative sums of input samples:
$x_k = a^r x_{k-r} + b(\, a^{r-1}(u_{k-r+1} + \ldots + u_k) + (a^{r-2} - a^{r-1})(u_{k-r+2} + \ldots + u_k) + \ldots + (a^1 - a^2)(u_{k-1} + u_k) + (a^0 - a^1)u_k\,)$,
$x_k = a^r x_{k-r} + b(\, r(a^{r-1})u_{k/r} + (r-1)(a^{r-2} - a^{r-1})u_{k/(r-1)} + \ldots + 2(a^1 - a^2)u_{k/2} + 1(a^0 - a^1)u_{k/1}\,)$.
From (9), $y_k = ca^r x_{k-r} + cbr(a^{r-1})u_{k/r} + cb\sum_{q=1}^{r-1} q(a^{q-1} - a^q)u_{k/q}$. As $0 < a < 1$, $\forall q \geq 1, (a^{q-1} - a^q) > 0$. Moreover, $b \geq 0$, $c \geq 0$, and the characterization $\lambda_q(u)$ ensures from (5)-(7) that $\forall q \in Q$, $\forall k \geq q$, $|u_{k/q}| \leq \lambda_q(u)$ (or, equivalently, $u_{k/q} \in 0 \pm \lambda_q(u)$) where $|.|$ is the absolute value operator. Notice that $k \geq q$ comes from $k \in \mathbb{N}$ in the statement of proposition 1. Then, a basic use of interval arithmetic gives: $y_k \in 0 \pm (ca^r \mu_{k-r} + cbr(a^{r-1})\lambda_r(u) + cb\sum_{q=1}^{r-1} q(a^{q-1} - a^q)\lambda_q(u))$.

Proof. Corollary 2
The proof of corollary 2 is based on the fact that a first order filter in $\mathbb{R}$ presents no overshoot. Therefore, if its state initial condition lies between the range of its input (as in $\mu_{k-r} = \lambda_1(u)$), the output will necessary remain in the same range. Since $c = 1$, the filter state x_k and the filtered output y_k are the same in this corollary. Therefore, provided the filter state initial condition $\mu_0 = \lambda_1(u)$ is fulfilled (which is easily satisfied in practice by simply choosing $x_0 = u_0$), direct applications of proposition 1 give the result stated in the corollary.

Proof. Proposition 3
The following preliminary remark is needed: $\forall(w,s) \in \mathbb{R}^n \times [-1,+1]^n$, $\exists\sigma \in [-1,+1]$, $w^T s = |w|\mathbf{1}\sigma$, where $|.|$ is the element-by-element absolute value operator and $\mathbf{1}$ is a column vector of 1s with appropriate size.(Proof: $s = -sign(w)$ and $s = +sign(w)$ give the extremal values possibly reached by $w^T s \in \mathbb{R}$).

Now, let $g_k^{\square} \in [-1,+1]$ denote a normalized bounded variable related to $g_k \in g_k^c \pm g_k^r$ so that the constraint $g_k = g_k^c + g_k^r g_k^{\square}$ is always satisfied. Similar notations are used for each bounded variable, $h_k = h_k^c + h_k^r h_k^{\square}$, etc. Proof by induction: assuming $x_k = x_k^c + x_k^r x_k^{\square}$ which is true at $k=0$, $x_{k+1} = g_k x_k + (1-g_k)h_k u_k$ can be firstly rewritten as: $x_{k+1} = (g_k^c + g_k^r g_k^{\square})(x_k^c + x_k^r x_k^{\square}) + (1 - g_k^c - g_k^r g_k^{\square}))(h_k^c + h_k^r h_k^{\square})u_k$ and, after simple rearrangements: $x_{k+1} = (g_k^c x_k^c + (1-g_k^c)h_k^c u_k) + g_k^c x_k^r x_k^{\square} + g_k^r x_k^c g_k^{\square} + g_k^r x_k^r g_k^{\square} x_k^{\square} + (1-g_k^c)h_k^r u_k h_k^{\square} - g_k^r h_k^c u_k g_k^{\square} - g_k^r h_k^r u_k g_k^{\square} h_k^{\square}$. Then, a factorization wrt uncertain monomes gives: $x_{k+1} = (g_k^c x_k^c + (1-g_k^c)h_k^c u_k) + ((g_k^c x_k^r)x_k^{\square} + (g_k^r x_k^c - g_k^r h_k^c u_k)g_k^{\square} + (g_k^r x_k^r)g_k^{\square} x_k^{\square} + (1-g_k^c)h_k^r u_k h_k^{\square} - (g_k^r h_k^r u_k)g_k^{\square} h_k^{\square})$. Applying the given remark with $w_k = [(g_k^c x_k^r), g_k^r(x_k^c - h_k^c u_k), (g_k^r x_k^r), (1-g_k^c)h_k^r u_k, -(g_k^r h_k^r u_k)]^T$ and $s_k = [x_k^{\square}, g_k^{\square}, (g_k^{\square} x_k^{\square}), h_k^{\square}, (g_k^{\square} h_k^{\square})]^T$ gives $x_{k+1} = x_{k+1}^c + x_{k+1}^r \sigma_k$ where x_{k+1}^c and $x_{k+1}^r = |w_k|\mathbf{1}$ are respectively given by (14) and (15), and where $\sigma_k \in [-1,+1]$ ensures the inclusion property (16) at time $k+1$. It can be noticed that (15) holds true thanks to the positivity of all interval radii and, also, that $x_{k+1}^r \geq 0$ since $|w_k|\mathbf{1} \geq 0$. A guaranteed inclusion is preserved wrt the specified model and a condition ensuring the stability of the (here, unidirectionally) coupled center and radius dynamics is $|g_k^c| + g_k^r < 1$: As $g_k^r \geq 0$, this condition implies $|g_k^c| < 1$ which first ensures the stability of the only center dynamics (14). Then, under a bounded input u_k, x_k^c is bounded and so is the whole input term of the radius dynamics (15). By considering $\check{x}_{k+1}^r = (|g_k^c| + g_k^r)\check{x}_k^r$ (homogenous discrete Linear Time-Varying (LTV) difference equation related to the radius dynamics), and by choosing $\mathcal{V}_k = (\check{x}_k^r)^2$ as Lyapunov function, it comes: $\Delta\mathcal{V}_k = \mathcal{V}_{k+1} - \mathcal{V}_k = ((|g_k^c| + g_k^r)^2 - 1)(\check{x}_k^r)^2$. So $\Delta\mathcal{V}_k < 0$ when $\check{x}_k^r \neq 0$ and $\Delta\mathcal{V}_k = 0$ when $\check{x}_k^r = 0$. This completes the proof of proposition 3.

REFERENCES

Aughenbaugh, J.M. and Paredis, C.J.J. (2006). Why are intervals and imprecision important in engineering design? In *REC2006, Reliable Engineering Computing Workshop*. Savannah, GA, USA.

Combastel, C. (2013). Stable interval observers in c for linear systems with time-varying input bounds. *IEEE Transactions on Automatic Control*, 58(2), 481–487.

Ding, S. (2008). *Model-based Fault Diagnosis Techniques*. Design Schemes, Algorithms, and Tools. Springer, Heidelberg, Berlin.

Efimov, D., Zolghadri, A., and Raïssi, T. (2011). Actuators fault detection and compensation under feedback control. *Automatica*, 47(8), 1699–1705.

Gheorghe, A., Zolghadri, A., Cieslak, J., Goupil, P., Dayre, R., and Berre, H.L. (2013). Toward model-based approaches for fast and robust fault detection in aircraft control surface servo-loop: From theory to application. *IEEE Control Systems Magazine*.

Goupil, P. (2010). Oscillatory failure case detection in the A380 electrical flight control system by analytical redundancy. *Control Engineering Practice*, 18, 1110–1119. doi:10.1016/j.conengprac.2009.04.003.

Goupil, P. (2011). Airbus state of the art and practices on fdi and ftc in flight control system. *Control Engineering Practice*, 19, 524–539.

Gouzé, J.L., Rapaport, A., and Hadj-Sadok, M.Z. (2000). Interval observers for uncertain biological systems. *Ecological Modeling*, 46–56.

Han, Y., Oh, S., Choi, B., Kwak, D., Kim, H., and Kim, Y. (2012). Fault detection and identification of aircraft control surface using adaptive observer and input bias estimator. *Control Theory & Applications, IET*, 6(10), 1367–1387.

Henry, D., Zolghadri, A., Cieslak, J., and Efimov, D. (2011). Fault detection and diagnosis in electrical aircraft flight control system. In *AIAA Guidance, Navigation and Control Conference (GNC'11)*. Portland, Oregon, USA.

Hwang, I., Kim, S., Kim, Y., and Seah, C.E. (2010). A survey of fault detection, isolation, and reconfiguration methods. *IEEE Transactions on Control Systems Technology*, 18(3), 636–653.

Kim, S., Choi, J., and Kim, Y. (2008). Fault detection and diagnosis of aircraft actuators using fuzzy-tuning imm filter. *IEEE Trans. Aerosp. Electron. Syst.*, 44(3), 940–952.

Mazenc, F. and Bernard, O. (2011). Interval observers for linear time-invariant systems with disturbances. *Automatica*, 47, 140–147.

Mazenc, F., Kieffer, M., and Walter, E. (2012). Interval observers for continuous-time linear systems with discrete-time outputs. *American Control Conference*, 1889–1894.

Raïssi, T., Efimov, D., and Zolghadri, A. (2012). Interval state estimation for a class of nonlinear systems. *IEEE Transaction Automatic Control*, 57(1), 260–265.

Raka, S. and Combastel, C. (2013). Fault detection based on robust adaptive thresholds: A dynamic interval approach. *Annual Reviews in Control*, 37(1), 119–128.

Vanek, B., Szabo, Z., Edelmayer, A., and Bokor, J. (2011). Geometric lpv fault detection filter design for commercial aircraft. In *AIAA Guidance, Navigation and Control Conference (GNC'11)*. Portland, Oregon, USA.

Varga, A., Hecker, S., and Ossmann, D. (2011). Diagnosis of actuator faults using lpv-gain scheduling techniques. In *AIAA Guidance, Navigation and Control Conference*. Portland, Oregon, USA.

Zolghadri, A. (2012). Advanced model-based fdir techniques for aerospace systems: Today challenges and opportunities. *Progress in Aerospace Sciences, Elsevier*, 18–29. Review article.

Zolghadri, A., Henry, D., Cieslak, J., Efimov, D., and Goupil, P. (2013). *Fault Diagnosis and Fault-Tolerant Control and Guidance for Aerospace Vehicles, from theory to application*. Series: Advances in Industrial Control. Springer.